IPST Technical Paper Series Number 572

Free Edge Flutter Based on 3-D Structural Characteristics of Paper

D. Qi and C.K. Aidun

May 1995

Submitted to
Journal of Pulp and Paper Science
and
TAPPI Engineering Conference
September 11–14, 1995
Dallas, Texas

Free Edge Flutter Based on 3-D Structural Characteristics of Paper

Dewei Qi[1] Cyrus K. Aidun[2]

Abstract

In order to study the effects of the microstructure of sheets at the onset of fluttering, we have added a 3-D angular distribution function to Cox's structural model of sheets. This makes it possible to predict the critical speed of air flows for the onset of fluttering in terms of single fiber properties, z-directional orientation of the fibers, and voids in the sheet. As an initial analysis, we assume air flow irrotational and make use of potential theory. Based on this analysis, the critical speed of air for sheet fluttering decreases as z-directional orientation of fibers increases, and the critical speed decreases as porosity increases and the fiber length decreases.

[1]Postdoctoral Research Fellow, School of Mechanical Engineering, Georgia Institute of Technology, Atlanta, Georgia 30318

[2]Associate Professor, Institute of Paper Science and Technology and School of Mechanical Engineering, Georgia Institute of Technology, Atlanta, Georgia 30318

Keywords

SHEET FLUTTER, FLUID DYNAMICS, WEB HANDLING, PAPER STRUCTURE, ANGULAR DISTRIBUTION FUNCTION, FIBER ORIENTATION.

1 Introduction

In a high-speed paper machine, air flows strongly interact with paper and cause the paper to vibrate in an out-of-plane direction. The vibration or flutter normally causes quality and runnability problems. If these problems are severe enough, then the possibility of crease and breaking greatly increases.

Fundamental knowledge and understanding of the interaction between sheets of paper and air will lead to a better design for transport of paper through the paper machine and reduce web breaks. Mujumdar and Douglas [1] have investigated the dynamic instability of sheets by using a threadline model. Later, Pramila [2] modified the model by adding additional mass due to the boundary layer of surrounding air. Chang and Moretti [3] incorporated the potential flow theory into the model to estimate the added mass. Wind

tunnel experiments have been conducted by Chang and Moretti [4] to seek the critical speed of air flows under different conditions. When the tension of the sheets is much larger than stiffness, the effect of the structure of sheets on flutter is neglected. However, when sheets are thick enough and tension is small, the effects of the structure of sheets at flutter become significant, particularly at the free edges.

In order to study the effects of sheet structure at the onset of sheet fluttering, a 3-D angular distribution function has been introduced into Cox's model [5]. Then, critical speeds of air flows for onset of fluttering have been predicted in terms of single fiber properties, z-directional orientation of the fibers, and voids.

2 Free edge flutter of the paper

The motion of a web or sheet in air can be described by the following equation,

$$m\frac{\partial^2 w}{\partial t^2} + 2mV\frac{\partial^2 w}{\partial x \partial t} + (mV^2 - T)\frac{\partial^2 w}{\partial x^2} + D[\frac{\partial^4 w}{\partial x^4} + 2\frac{\partial^4 w}{\partial y^2 \partial x^2} + \frac{\partial^4 w}{\partial y^4}] = p^- - p^+ \tag{1}$$

where m is the mass per unit area of web, w is the displacement in the z (thickness) direction, t is the time, V is the velocity of moving web, T is the tension of web, D is the bending stiffness of the web, and the term $p^- - p^+$ is the aerodynamic pressure difference between the the top and bottom surfaces of the sheet. In sheet flutter experiments inside a wind tunnel, where the velocity of the sheet is equal to zero, this equation reduces to

$$m\frac{\partial^2 w}{\partial t^2} - T\frac{\partial^2 w}{\partial x^2} + D[\frac{\partial^4 w}{\partial x^4} + 2\frac{\partial^4 w}{\partial x^2 \partial y^2} + \frac{\partial^4 w}{\partial y^4}] = p^- - p^+ \tag{2}$$

The stiffness D is given by

$$D = Eh^3/12(1-\nu) \tag{3}$$

where E is Young's modulus of the sheet, h is the thickness of sheet, and ν is Poisson's ratio. If tension T is much larger than D, the term with the fourth-order derivatives can be negligible. However, when the sheet is stretched by using a uniform force at the ends, the stress distribution in the sheet is not uniform. The tension close to the free edges becomes very small. This can be easily confirmed by simple finite-element analysis. The free edge effects may cause large-amplitude flutter of the sheet at low critical speed. The dynamic instability and its important effect have been investigated by Chang and Moretti [4]. However, they did not consider the effects of the microstructure of the sheet on the onset of sheet flutter. In our work, we analyze the effects of the microstructure of the sheet, such as voids, z-directional orientation of fibers, and single-fiber properties on the dynamic stability of the sheet. A model of the microstructure of the fiber network is first introduced in the following section.

3 Microstructure of paper

3.1 3-D angular distribution function

Paper is made of a three-dimensional random fiber network. Macromechanical properties of the paper, such as elastic constants, $C_{\alpha\beta\nu\mu}$, depend essentially on properties of a single fiber and its distribution in space. Angular distribution function $f(theta, \phi)$ can be defined as the possibility of finding a fiber per unit solid angle at polar angle (θ, ϕ) (see Figure 1). Thus,

$$f(\theta, \phi) = \frac{1}{n} \sum_i \delta(cos\theta - cos\theta_i)\delta(\phi - \phi_i), \tag{4}$$

where δ is the Dirac delta function, n is the total number of fibers, subscript i indicates the ith fiber in the system. The angular distribution function may be expanded in the series of spherical harmonic functions in real number space,

$$f(\theta, \phi) = \sum_{l=0}^{l=\infty} \sum_{m=0}^{m=l} [Q^c_{lm} Y^c_{lm}(\theta, \phi) + Q^s_{lm} Y^s_{lm}(\theta, \phi)], \tag{5}$$

where Y^c_{lm} is defined as

$$Y^c_{lm} = P_{lm}(cos\theta) C_m(\phi) \tag{6}$$

and

$$Y_{lm}^{s} = P_{lm}(cos\theta)S_m(\phi) \tag{7}$$

with

$$C_m(\phi) = \frac{1}{\sqrt{\pi}} cosm\phi, \quad m \neq 0$$

$$C_0 = \frac{1}{\sqrt{2\pi}},$$

$$S_m(\phi) = \frac{1}{\sqrt{\pi}} sinm\phi.$$

Q_{lm}^{c} and Q_{lm}^{s} are expansion coefficients. $P_{lm}(cos\theta)$ is a normalized Associated Legendre function; l and m are the integers. Substituting equation (4) into (5), multiplying it by Y_{lm}^{c} or Y_{lm}^{s}, integrating both sides of this equation, and making use of the orthogonality properties of the basis functions, we get

$$Q_{lm}^{c} = \frac{1}{n} \sum_{i} P_{lm}(cos\theta_i)C_m(\phi_i), \tag{8}$$

and

$$Q_{lm}^{s} = \frac{1}{n} \sum_{i} P_{lm}(cos\theta_i)S_m(\phi_i).$$

Because of the orthogonality of harmonic functions, the terms with l larger than 4 do not contribute any physical property to the paper. Therefore,

we can truncate the series at $l = 4$. Furthermore, if a symmetrical invariance of inversion for the fiber network is imposed, we can delete all odd l terms because the parity of the spherical harmonic functions is l. Assuming that the fiber-orientational distribution is symmetric with respect to the mid-plane, machine direction, and crossmachine direction of the sheet, we drop all terms which contain $sinm\phi$ (we can drop the s in coefficient Q^s_{lm} and c in Q^c_{lm} from now on). Therefore, the 3-D angular distribution function for machine-made paper is proposed as

$$\begin{aligned} f(\theta,\phi) &= \frac{1}{4\pi} + Q_{20}P_{20}(cos\theta)C_0 + Q_{40}P_{40}(cos\theta)C_0 + Q_{22}P_{22}(cos\theta)C_2(\phi) \\ &+ Q_{42}P_{42}(cos\theta)C_2(\phi) + Q_{44}P_{42}(cos\theta)C_4(\phi). \end{aligned} \tag{9}$$

Five independent coefficients are required to describe the distribution of fibers in a 3-D space; we will address these in future reports.

If we focus on how z-directional distribution of fibers affects the in-plane mechanical properties of paper, and assume the distribution of fibers is isotropic in the x-y plane, such as handsheets, then the angular distribu-

tion function is reduced to a simpler form, given by

$$f(\theta,\phi) = \frac{1}{4\pi} + Q_{20}P_{20}(cos\theta)C_0 + Q_{20}P_{40}(cos\theta)C_0. \qquad (10)$$

In order to use the orthogonality of spherical harmonic functions, we have normalized $f(\theta,\phi)$ to 1 by integrating θ from 0 to π and ϕ from 0 to 2π. In this way, we have moved the end point of the fiber to the origin of the coordinate system to determine the angular distribution function. Mechanical property, say B, is calculated by

$$< B >= \frac{\int_0^{\pi}\int_0^{2\pi} Bf(\theta,\phi)sin\theta d\phi d\theta}{\int_0^{\pi}\int_0^{2\pi} f(\theta,\phi)sin\theta d\phi d\theta} = \frac{\int_0^{\frac{\pi}{2}}\int_0^{2\pi} Bf(\theta,\phi)sin\theta d\phi d\theta}{\int_0^{\frac{\pi}{2}}\int_0^{2\pi} f(\theta,\phi)sin\theta d\phi d\theta}$$

. The final results for mechanical properties should not depend on the way of normalizing $f(\theta,\phi)$. The second equality in the above equation is a simple consequence of the angular symmetry of the distribution function.

3.2 Structural model of paper

Using a model of 3-D sheets, proposed by Cox [5], and the 3-D angular distribution function introduced above, we may predict the anisotropic properties of the sheet. If the sheet is under tensile strain $e_{\alpha,\beta}$, the strain along a fiber

with polar angle (θ, ϕ) is given by

$$\begin{aligned} e_f &= sin^2\theta cos^2\phi e_{xx} + sin^2\theta sin^2\phi e_{yy} + cos^2\theta e_{zz} \\ &+ sin^2\theta cos\phi sin\phi e_{xy} + sin\theta cos\theta cos\phi e_{xz} + sin\theta cos\theta sin\phi e_{yz}, \end{aligned} \quad (11)$$

where engineering strains are employed. The energy density W can be written as

$$\begin{aligned} W &= \frac{1}{2}\int_0^{\pi}\int_0^{2\pi} \sigma_f e_f V_f N f(\theta,\phi) sin\theta d\theta d\phi \\ &= \frac{1}{2}\int_0^{\pi}\int_0^{2\pi} E_f(1-\Omega) e_f^2 f(\theta,\phi) sin\theta d\theta d\phi \end{aligned} \quad (12)$$

where σ_f is the stress on the fiber, V_f represents the volume of a single fiber, N is the total number of fibers per unit volume, and Ω is the porosity of the sheet. All elastic constants of the sheet can be calculated from

$$\sigma_{\alpha\beta} = \frac{\partial W}{\partial e_{\alpha\beta}} = C_{\alpha\beta\mu\nu} e_{\mu\nu}, \quad \alpha, \beta = x, y, z \quad (13)$$

where $\sigma_{\alpha\beta}$ is the stress tensor, and $C_{\alpha\beta\nu\mu}$ is the elastic constant tensor.

The elastic constants required for this study are given by

$$\begin{pmatrix} C_{xxxx} & C_{xxyy} & C_{xxzz} \\ & C_{yyyy} & C_{yyzz} \\ & & C_{zzzz} \end{pmatrix}$$

with

$$C_{yyyy} = C_{xxxx} = K(\frac{1}{5} - \frac{4\sqrt{5\pi}}{35}Q_{20} + \frac{2\sqrt{\pi}}{35}Q_{40}) \tag{14}$$

$$C_{xxyy} = K(\frac{1}{15} - \frac{4\sqrt{5\pi}}{105}Q_{20} + \frac{2\sqrt{\pi}}{105}Q_{40}) \tag{15}$$

$$C_{xxzz} = C_{yyzz} = K(\frac{1}{15} + \frac{2\sqrt{5\pi}}{105}Q_{20} - \frac{8\sqrt{\pi}}{105}Q_{40}) \tag{16}$$

$$C_{zzzz} = K(\frac{1}{5} + \frac{8\sqrt{5\pi}}{35}Q_{20} + \frac{16\sqrt{\pi}}{105}Q_{40}) \tag{17}$$

where $K = E_f(1-\Omega)$. If paper is completely isotropic in 3-D space, then all $Q_{lm}^{c,s}$ are zero except Q_{00}, and the above results for C are correctly obtained for this case as expected. The relation between normal stress tensor σ and normal strain tensor $\mathbf{e}$ can be expressed as a matrix form, $\sigma = C\mathbf{e}$ or $\mathbf{e} = C^{-1}\sigma$. Therefore, Young's modulus E and Poisson's ratio ν of the sheet in equation (3) are obtained by

$$E = \frac{1}{(C^{-1})_{xxxx}} \tag{18}$$

$$\nu = -\frac{(C^{-1})_{xxyy}}{(C^{-1})_{xxxx}} \tag{19}$$

3.3 Finite fiber-length model

When fibers are short and the fiber "end effect" cannot be neglected, we have to use a finite fiber-length model. Let us consider a single fiber with finite length l_0 embedded in the fiber network where fibers are bonded together. Assume that the fiber is rod-like with radius r_0, and the mean separation of the fibers normal to their length is r_1. If the fiber network (sheet) is subjected to strain $e_{\alpha\beta}$, then strain e_s in the sheet along the fiber direction at a distance r_1 from the fiber centroid is governed by the same equation as in (11) except e_f is replaced by e_s. Shear stress τ may transfer from the fiber surrounding to the fiber. We can balance the shear forces in the network with the shear forces at the interface of the fiber and the network, where shear stress is τ_0, that is

$$2\pi r\tau d\xi = 2\pi r_0\tau_0 d\xi,$$

where $d\xi$ is an infinitesimal segment of the fiber. Using $\tau = Gdu/dr$, where du/dr is the shear strain and G is the mean shear transfer constant, we obtain

$$\frac{du}{dr} = \frac{r_0\tau_0}{G}\frac{1}{r}.$$

After integrating the above equation from r_0 to r_1, we have

$$\tau_0 = \frac{G}{r_0 ln\frac{r_1}{r_0}}(u_s - u_f),$$

where u_s is the displacement of the fiber network along the fiber direction at r_1, and u_f is the axial displacement of the fiber. Balancing the shear forces at the interface with the tensile force in the fiber, we can write

$$dF + 2\pi r_0\tau_0 d\xi = 0.$$

Using the above two equations, we can write

$$\frac{d^2F}{d\xi^2} + H(e_s - \frac{1}{E_fA}F) = 0$$

where $e_s = du_s/d\xi$ has been used, A is the cross-sectional area of the fiber, F is the tensile force on the fiber, and $H = \frac{2\pi G}{ln(r_1/r_0)}$. The solution to the

equation, considering boundary conditions $F = 0$ at $\xi = 0$ and $\xi = l_0$, is given by

$$F = E_f A e_s [1 - \frac{ch\lambda_0(l_0/2 - \xi)}{ch\frac{\lambda_0 l_0}{2}}],$$

where $\lambda_0 = \sqrt{H/E_f A}$ and l_0 is the fiber length. The energy density, W_1, due to tensile stresses can be calculated following the same procedure as those in section 2.2. The result is given by

$$\begin{aligned} W_1 &= \frac{1}{2} A E_f N \int_0^{l_0} \int_0^{\pi} \int_0^{2\pi} e_s^2 [1 - \frac{ch\lambda_0(l_0/2 - \xi)}{ch\frac{\lambda_0 l_0}{2}}]^2 f(\theta, \phi) sin\theta d\theta d\phi d\xi \\ &= \frac{1}{2} A E_f N (l_0 - \frac{3}{\lambda_0} th\frac{\lambda_0 l_0}{2} + \frac{2}{2ch^2\frac{\lambda_0 l_0}{2}}) \int_0^{\pi} \int_0^{2\pi} e_s^2 f(\theta, \phi) sin\theta d\theta d\phi \quad (20) \end{aligned}$$

The energy density W_2 due to shear stress transmitted is, similarly, given by

$$\begin{aligned} W_2 &= \frac{1}{2} N \int_0^{l_0} \int_{r_0}^{r_1} \tau \frac{du}{dr} 2\pi r dr d\xi \int_0^{\pi} \int_0^{2\pi} f(\theta, \phi) sin\theta d\theta d\phi \\ &= \frac{1}{2} A E_f N \int_0^{l_0} \int_0^{\pi} \int_0^{2\pi} e_s^2 \frac{sh^2\lambda_0(l_0/2 - \xi)}{ch^2\frac{\lambda_0 l_0}{2}} f(\theta, \phi) sin\theta d\theta d\phi d\xi \\ &= \frac{1}{2} A E_f N (\frac{th\frac{\lambda_0 l_0}{2}}{\lambda_0} - \frac{l_0}{2ch^2\frac{\lambda_0 l_0}{2}}) \int_0^{\pi} \int_0^{2\pi} e_s^2 f(\theta, \phi) sin\theta d\theta d\phi. \end{aligned}$$

Total energy is written as

$$W = W_1 + W_2 = \frac{1}{2} E_f (1-\Omega)(1 - \frac{th\frac{\lambda_0 l_0}{2}}{\lambda_0 l_0/2}) \int_0^{\pi} \int_0^{2\pi} e_s^2 f(\theta,\phi) sin\theta d\theta d\phi.$$

Final results for elastic constants are similar to equations (14) (15) (16) (17), where K is now replaced by $E_f(1-\Omega)(1 - \frac{th\frac{\lambda_0 l_0}{2}}{\lambda_0 l_0/2})$ for the finite fiber length model. We have used $\lambda_0 = 0.04(m)^{-1}$ as in reference 5 for later calculation.

4 Analysis of flutter

Chang and Moretti [3,4] have conducted wind tunnel experiments to investigate the free edge flutter. In their experiments, tension is applied across flow direction. They analyze and predict the dynamic instability for the free edge fluttering by using potential flow theory. We briefly review their procedure here and refer the reader to the reference [4] for more details. The air flow is assumed to be two-dimensional in their analysis. The aerodynamic pressure on the sheet is expressed by the inviscid flow equation, given by

$$p_{\pm} = -\rho[\frac{\partial \varphi}{\partial t} + V\frac{\partial \varphi}{\partial y}]_{z=0\mp}$$

where φ is the flow potential, y is in the primary flow direction, and ρ is the density of air. The deflection of the sheet can be assumed to follow

$$w = \hat{w}cos(\frac{\pi x}{L})e^{i(\omega t - \kappa y)}$$

where $\hat{w}$ is the amplitude of vibration, L is the length of the paper tested, and κ is a wave length. Boundary conditions for step change in pressure across the sheet are given by

$$p_+ - p_- = 2p_+$$

and

$$p_+ = -\rho\hat{w}\frac{(\omega - \kappa V)^2}{\kappa}e^{i(\omega t - \kappa y)}.$$

Therefore, the governing equation becomes

$$-\omega^2 m + D[(\pi/L)^2 + \kappa^2]^2 + (\pi/L)^2 T\hat{w}e^{i(\omega x - \kappa y)} - 2\rho\hat{w}e^{i(\omega - \kappa y)}(\omega - \kappa V)^2/\kappa = 0$$

where the x-dependent term $cos(\pi x/L)$ is dropped because of the 2-dimensional flow assumption. The characteristic equation is given by

$$(m + \frac{2\rho}{\kappa})\omega^2 - 4\rho V\omega + 2\kappa\rho V^2 - D[(\pi/L)^2 + \kappa^2]^2 - (\pi/L)^2 T = 0.$$

From this quadratic equation, the frequency can be written as

$$\omega = \frac{4\rho V \mp \sqrt{(4\rho V)^2 - 4(m + 2\rho/\kappa)2\kappa\rho V^2 - D[(\pi/L)^2 + \kappa^2]^2 - (\pi/L)^2 T}}{2(m + \rho/\kappa)}.$$

The stability boundary equation is given by

$$\rho V^2 - \frac{1}{2\kappa}(1 + 2\rho/m\kappa)D[(\pi/L)^2 + \kappa^2]^2 + 92\pi/L)^2 = 0, \qquad (21)$$

where $\kappa = 2\pi/\lambda$, and

$$\lambda = 2L([\frac{TL^2}{\pi^2 D} + 1]^{-\frac{1}{4}}.$$

The critical flow speed V_c and critical dynamic pressure q_c can be calculated from equation (21), and flutter frequencies above the critical speed are given by

$$f_0 = \frac{V}{\lambda + \pi m/\rho}.$$

The elastic modulus E and Poisson ratio ν can be evaluated from equations (18) and (19) based on the structural model of the sheet. For $m = 0.058kg/m^2$ and $L = 0.23m$, the stiffness D in terms of E and ν may vary with parameter tension T, porosity Ω, single fiber modulus E_f, and z-dimensional

angular distribution, respectively. Critical speed for edge fluttering and respective frequencies can be obtained as a function of paper's structural and physical properties.

First, we consider three cases corresponding to different z-directional orientation of fibers. In case A, fibers are uniformly distributed in the 3-D space; in turn, Q_{20} and Q_{40} in equation 10 are zero. In case B, fiber orientation is symmetric in the x-y plane; Q_{20} and Q_{40} in equation 10, which represent the anisotropic distribution in the z-direction, are fitted to the curve in Figure 8 of reference 6, which is a projection of z-directional distribution on the x-z plane, based on experiments by Hasuike et al. [6] (we have re-normalized the curve). In this case, Q_{20} and Q_{40} are -0.08803 and 0.06307, respectively. Case C is constructed by setting $Q_{20} = -0.120$ and $Q_{40} = 0.073$ in equation 10. The degree of z-directional orientation of fibers in case A is larger than in case B, and smallest in case C. This is because Q_{20} is essentially the statistical average of $P_{20}(x_i)$ (see equation 8), where $x_i = cos(\theta_i)$, of all fibers, and the value of $P_{20}(x)$ increases monotonically with the absolute value of x

(see Figure 2). Therefore, Q_{20}, which is refered to as z-directional ordering parameter by us, can be used to measure the degree of z-directional orientation. Other parameters are fixed for these three cases as specified in Table 1. The single fiber modulus is selected as 77.3 GPa corresponding to chemical pulp according to references [7,8]. The calculation result for modulus of the sheet is 6.48 GPa, which is in good agreement with experimental results [9].

Table 1.

$m(kg/m^2)$	$T(N/m)$	$E_f(GPa)$	Ω	$L(m)$
0.058	10	77.3	0.60	0.23

The results of critical speeds and frequencies for cases A, B, and C are collected in Table 2. The critical air speeds are plotted against the z-directional ordering parameter Q_{20} in Figure 3. Since in this study we assume the flow to be irrotational, the critical dynamic pressure is given as $q_c = \frac{1}{2}\rho V_c^2$, where V_c is the critical speed of air. The critical air speed and fluttering frequency decrease as the z-directional ordering increases.

Table 2.

	Q_{20}	Q_{40}	$E(GPa)$	ν	$q_c(Pa)$	$V_c(m/s)$	f_0
case A	0.0	0.0	5.15	0.25	55.71	9.46	30.87
case B	-0.088	0.063	6.48	0.277	61.69	10.14	31.55
case C	-0.120	0.073	6.89	0.277	63.40	10.28	31.73

To investigate the effect of porosity at the onset of sheet flutter, the porosity Ω is set to different values, while Q_{20} and Q_{40} are the same as in case B. Other parameters are the same as those in Table 1. It is shown in Table 3 and Figure 4 that critical speed and frequency decrease as porosity increases. We can see that increasing voids has an adverse effect in terms of the dynamic stability of sheets in the paper machine.

Table 3.

	Ω	$E(GPa)$	$q_c(Pa)$	$V_c(m/s)$	f_0
case C	0.8	3.24	45.62	8.72	29.58
case D	0.7	4.86	54.26	9.51	30.70
case E	0.6	6.48	61.69	10.14	31.55
case F	0.4	9.72	74.46	11.14	32.85

Finally, critical speeds are calculated for fiber lengths from 0.05 mm to 2 mm, while other parameters have the same values as in case B. The results are presented in Table 4 and plotted in Figure 5. Only fibers shorter than

0.5 mm have adverse effects on the stability of sheets. The instability is not affected by fibers longer than 1 mm.

Table 4.

	$l_0(mm)$	$E(GPa)$	$q_c(Pa)$	$V_c(m/s)$	f_0
case G	0.05	1.54	33.44	7.48	27.68
case H	0.1	3.36	46.25	8.78	29.67
case I	0.5	5.83	58.93	9.91	31.23
case J	1.0	6.16	60.36	10.13	31.40
case K	2.0	6.32	61.08	10.09	31.47

In all calculations, tension T is set to $10N/m$. For smaller tension, the critical speed would become more sensitive to the sheet structure. The two-dimensional assumption, that is, $L >> \lambda$ used with potential theory, is applicable only for large tension. We are working on computational analysis of the full fluid flow equations to remove this and other restrictions from the analysis.

5 Conclusion

In order to analyze the effects of z-directional orientation of fibers on dynamic instability of sheet fluttering, a 3-D angular distribution function is proposed

in this study. Both Cox's microstructure model of sheet and potential theory for the fluid flow are used to predict the critical speed of air in terms of physical characteristics of the sheet, such as single fiber properties, porosity, and fiber orientation in the z-direction. It is found that critical speed decreases as the z-direction orientation of fibers increases and that critical speed decreases as porosity increases and the fiber length decreases.

Acknowledgements

This study is supported by the National Science Foundation under grant CTS-9258667 and industrial contributions.

REFERENCES

1. Mujumdar, A.S. and Douglas, W.J.M. *Sevensk Paperstid.* 79 (**6**): 187 (1976).

2. Pramila, A. *Sheet Flutter & Windage Problems Seminar TAPPI* notes, 22 (1991).

3. Chang, Y.B. and Moretti, P.M. *Sheet Flutter & Windage Problems*

Seminar. TAPPI notes, 14 (1991).

4. Chang, Y.B. and Moretti, P.M. *Web Handling*, ASME 67 (1992).

5. Cox, H.L., *British J. Appl. Phys.* **3**: 72 (1952).

6. Hasuike, M., Kawasaki, T., and Murakami, K. *J. Pulp and Paper Science*, **18** (3), J114 (1992).

7. Subramanian, L., Carlsson, L.A., *TAPPI* **77**:11, 209 (1994).

8. Page, D.H., El-Hosseiny, F., and Lancaster, A.P.S. *TAPPI* **64**:4, 114 (1977).

9. Baum, G.A., Brennan, D.C., and Habeger, C.C., *TAPPI* **64**(8) 97 (1981).

Caption of Figures

Figure 1. Coordinat system for fiber in a 3-D space.

Figure 2. $P_{20}(x)$ increases monotonically with the absolute value of $x = cos\theta$ while $P_{40}(x)$ does not.

Figure 3. The critical speed decreases as the z-directional ordering increases.

Figure 4. The critical speed decreases as porosity increases.

Figure 5. The relationship between critical speed and fiber length.

Fig. 1,

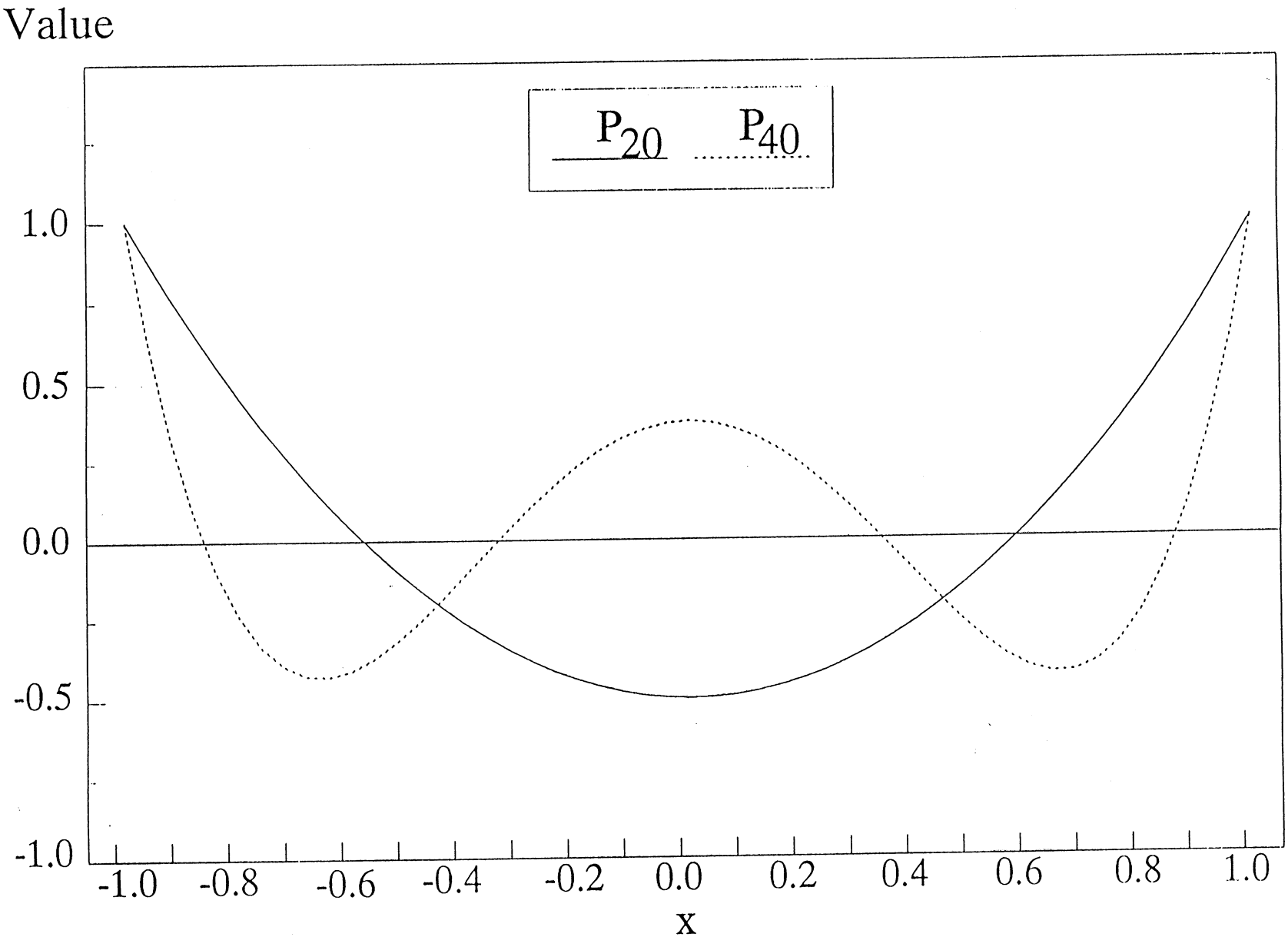

Fig. 2,

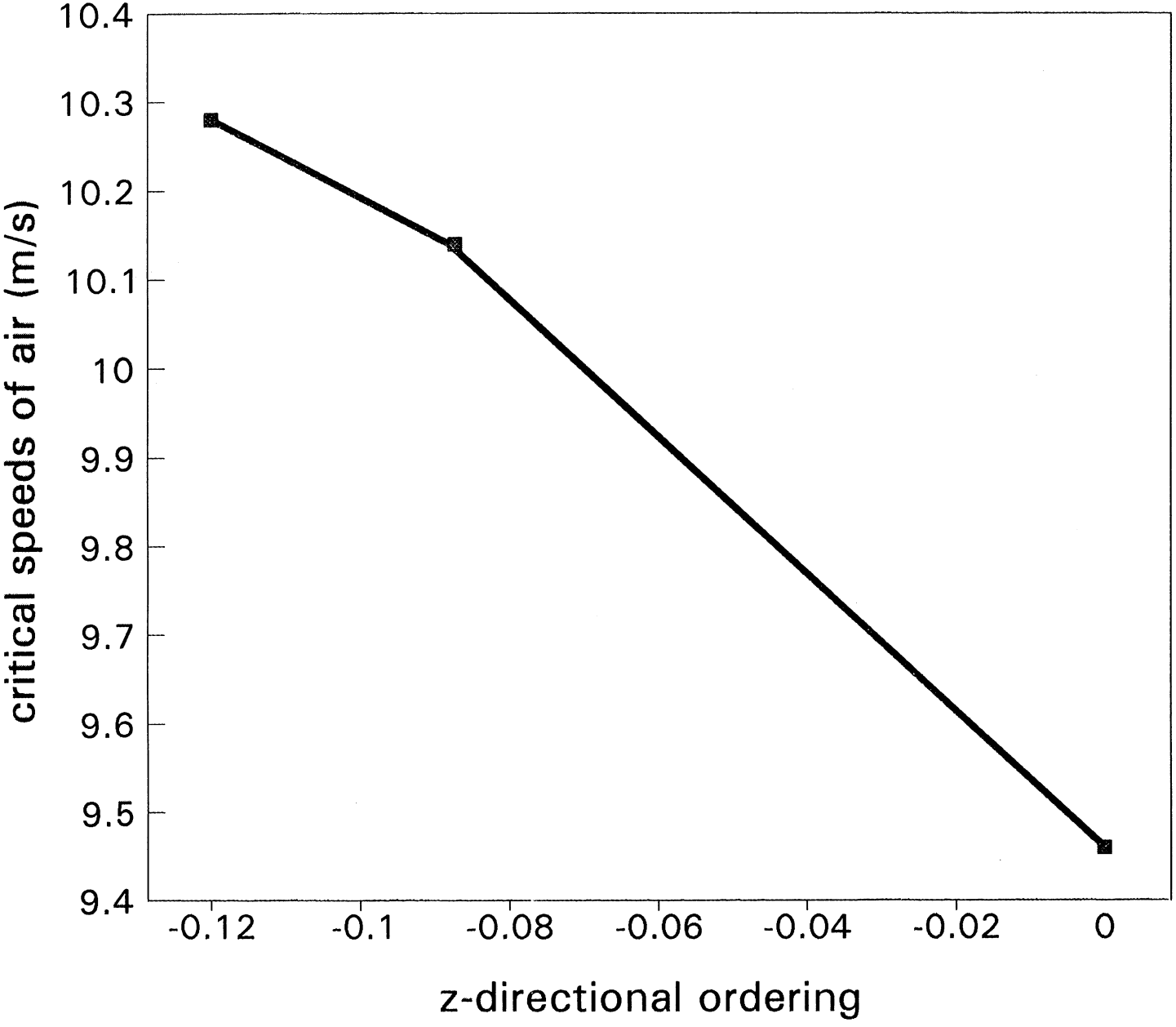
10.4
10.3
10.2
10.1
10
9.9
9.8
9.7
9.6
9.5
9.4
critical speeds of air (m/s)
-0.12
-0.1
-0.08
-0.06
-0.04
-0.02
0
z-directional ordering

Fig.3,

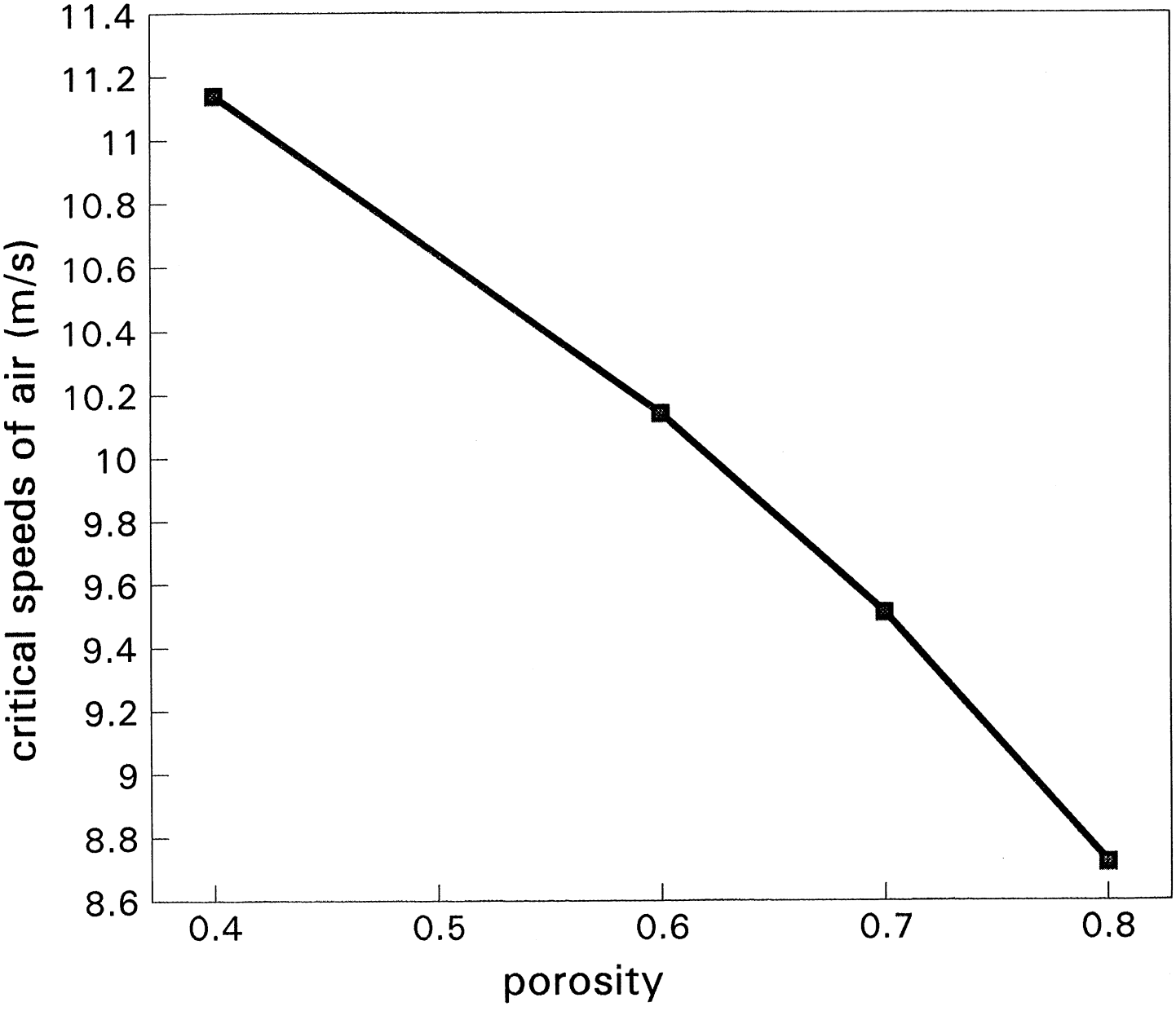
11.4
11.2
11
10.8
10.6
10.4
10.2
10
9.8
9.6
9.4
9.2
9
8.8
8.6
critical speeds of air (m/s)
0.4
0.5
0.6
0.7
0.8
porosity

Fig. 4,

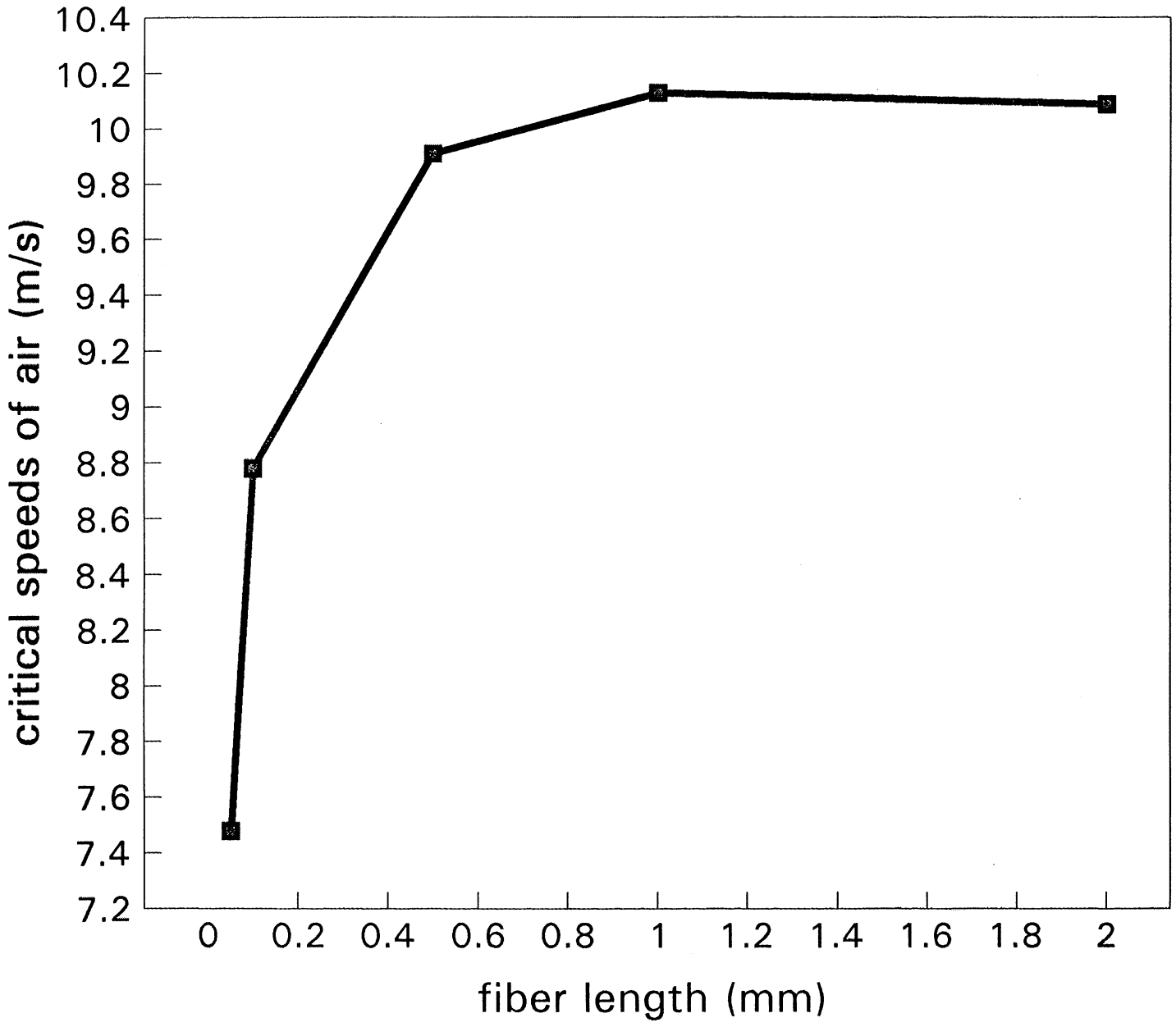
10.4
10.2
10
9.8
9.6
9.4
9.2
9
8.8
8.6
8.4
8.2
8
7.8
7.6
7.4
7.2
critical speeds of air (m/s)
0
0.2
0.4
0.6
0.8
1
1.2
1.4
1.6
1.8
2
fiber length (mm)

Fig. 5,